Considerations on the Electrode-Spacing-to-Electrode-Diameter Ratio in Electrical Resistivity Tomography (ERT): An Operational Approach

Lorenzo Ciani⬤, *Senior Member, IEEE*, Gabriele Patrizi⬤, *Member, IEEE*, Agnese Innocenti⬤, Riccardo Fanti⬤, and Veronica Pazzi⬤

Abstract— To develop small-scale, shallow, and high-resolution electrical resistivity surveys (e.g., for archeological or agricultural purposes), the available literature highlights few requirements in terms of distance between two adjacent electrodes or electrode's length embedded in the soil. Nevertheless, there are no studies about the influence of the electrode's diameter and/or the electrode's diameter-to-electrode spacing ratio. Thus, this work proposes to investigate this ratio in relatively small-scale surveys (electrode spacing from 10 to 100 cm) to define an operational approach. The analysis has been conducted comparing the apparent resistivity data acquired by means of electrodes different in terms of diameter and materials. The apparent resistivity was chosen to avoid the introduction of further errors/approximations caused by the inversion procedure. Overall, six different types of electrodes have been employed and tested. The results of the data analysis emphasize the necessity of taking into account the electrode's diameter-to-electrode spacing ratio in the case of small-case electrical resistivity tomography (ERT) surveys.

Index Terms— Electrical impedance tomography, electrodes, geophysical measurements, geophysics, soil measurements.

I. INTRODUCTION

NONINVASIVE geophysical techniques are indirect methods that detect the variations of the physical properties of the ground caused by the presence of anomalies [1]. The analysis and interpretation of these variations allow researchers to quantify and define these anomalies, i.e., define their sources, dimensions, and location. Among the well-known and widely used geophysical techniques, there is electrical resistivity tomography (ERT), a method that uses current and voltage data acquired on the surface to reconstruct the subsoil

resistivity variation [2], [3]. Resistivity (or its inverse called conductivity) is the capacity of the rock/soil materials to resist (facilitate, in the case of the conductivity) the passage of a current and it is influenced, among the other, by the degree of saturation and the fluid content, by temperature, lithology, and porosity [1].

This technique is commonly applied in different fields, e.g., hydrogeology [4], environmental investigation [5], natural hazard assessment [6], waste/residual investigation [7], agronomy [8], oil and gas [9], civil engineering [10], dredging engineering [11], and archeology [12]. Furthermore, ERT is commonly used also for the reconstruction of the resistivity of other objects instead of the soil. Few examples of these applications are two-phase flow measurements [13], [14] (where the measurand is a fluid in a pipe), vertical flow in pipeline measurements [15], biomedical engineering applications such as anatomical atlas [16], and conductive measurement of thin-film electronic devices [17].

To collect current and voltage data, four electrodes are commonly used arranged on the surface according to different layouts called "arrays" [18]. In the last 20 years, many authors have proven that the electrical potential in the subsoil, and thus, the acquired apparent resistivity data and, as a cascade effect, the inverted model are sensitive to the positions of the following:

1) the receivers, i.e., the voltage electrodes, which are usually called M and N (see for more details [12]);
2) the source, i.e., the current electrodes, which are usually called A and B (see for more details [12]).

In particular, a wrong deployment of the electrodes along the ERT line or the finite distance of the remote pole in the case of a pole-dipole (PD) array can generate artifact that can be interpreted as subsoil anomalies (see for instance [19], [20], [21], [22], [23]).

Another typology of error that can affect ERTs is the systematic one that cannot be removed by the averaging/staking of the data. These errors, e.g., the cable leakage or the active electrode length, in fact, are generated by the nonideal procedures or by the measurement systems [24], [25], [26]. Thus, this category of errors includes those caused by the electrodes themselves and in particular by the following:

1) the length of electrode embedded in the soil and thus considered "active" with respect to the current generation [26], [27];
2) the electrode material [2], [24];
3) the soil-electrode contact [25], [28].

The image reconstruction processes (also known as inversion algorithms) usually assume that the size of the electrodes is negligible compared to the distance "a" between two adjacent electrodes or the geometrical parameters of the employed model (i.e., electrodes are usually assumed to be ideal points). However, this assumption is not true, and artifacts can be generated if the part of the electrode embedded in the ground, i.e., the active electrode length, is too long compared to the "a" distance. In the case of long active electrodes, in fact, the model resolution decreases, and the signal-to-noise ratio increases with depth. When ERTs are applied to small-sized targets such as civil engineering and/or cultural heritage artifacts (e.g., diagnostic, management, and restoration or conservation of ancient handworks such as columns, walls, statues, pottery, and so on [2], [29]), or agricultural applications (e.g., understand the root–soil interactions or the temporal soil moisture variation in the first 30–40 cm of soil [8]), they are called small-scale ERT because of the miniaturized dimension of the targets [29]. In these applications, a high resolution at shallow depth is needed and it can be achieved thanks to a miniaturization of the instrumentation, which means electrodes with a diameter of few millimeters (e.g., steel nails) and the interelectrode distance "a" of few centimeters. In these applications, where the investigated volume is very small, the nonpunctiform shape of the electrode (i.e., its dimensions compared to the investigated volume itself), if not correctly considered, can generate artifacts [26], [30]. In literature, studies can be found, which suggests that if the ratio of active electrode length to "a" spacing is higher than 0.2 [27], a 3-D modeling of the electrodes is needed (e.g., the shunt-electrode model (SEM) or the complete electrode model (CEM) or the conductive cell model (CCM) as in [26] and [31] and references therein). Nevertheless, in [26], this has been demonstrated that, in micro-ERT profiles characterized by a high ratio of the active electrode length to electrode spacing "a," the 3-D modeling of the electrode can be avoided in favor of the approximation of the active electrode shape with an equivalent electrode point (EEP) located at 73% of the depth of the total electrode length. They also demonstrated that "a" should be higher than twice the active length and lower than the characteristic dimension of the shallow heterogeneity divided by 0.75 [26]. Ronczka et al. [31] investigate the use of boreholes as long electrodes and, thus, the influence of both different borehole's diameters. They proved that for electrodes with a high length-to-diameter ratio, the diameter to "a" spacing ratio should be lower than 1% to have numerical error less than 1%. Moreover, they demonstrated that combining electrodes of different lengths (e.g., boreholes and surface electrodes), it is possible to increase the reliability of results.

As it is well known, electrodes can be metal stakes or plates, and these last employed when/where it is difficult or not recommended (e.g., on archeological sites) to insert stakes in the soil/structure. Usually, they are made of stainless steel

and rarely other metals or graphite [32], [33]. In the past, non-polarizable electrodes were widely used to carry out induced polarization (IP) surveys to reduce the electric noise generated by the subsoils' self-potentials, but nowadays, they are commonly replaced by metal stakes that are more user-friendly with multielectrode tomography acquisitions [34]. Nevertheless, according to recent literature [24], [25], the research questions still open in ERT measurements that regard the relationship between systematic errors and the electrode type material, the history of use, and the voltage/current applied.

This work takes its cue from some needs that can be encountered in a geophysical measurement campaign that is not fully addressed in the available literature: first, the necessity to develop a parallel setup, but because of technical issues, there is not the possibility to use the same electrodes in terms of dimensions and materials, and on the other hand, to develop a shallow and high-resolution survey (e.g., for archeological or agricultural purposes) using available material. The latter means that electrodes specifically developed for the purposes of the small-scale survey (i.e., with a very small diameter [27] or gels or sponges) cannot be employed, while those with a diameter of some millimeters have to be used and placed at a relatively small distance (less than 50 cm) to each other.

Thus, the purpose of this work is to investigate the ratio between the interelectrode distance "a" and the electrode's diameter φ (the a/φ ratio) in a relatively small-scale survey to define an operational approach. The major contributions brought by this research are the following.

1) The introduction of an operational approach to estimate the impact of the electrode's diameter in small-scale ERT surveys.
2) The definition of a range of applicability of electrodes as a function of the electrode spacing to electrode's diameter a/φ ratio to avoid possible artifacts in the presence of resistive targets.
3) The proof that the materials used (different types of stainless-steel and carbon electrodes) have no particular effect in the measured resistivity.
4) The analysis also pointed out the major impact of inadequate a/φ that can be seen in the case of subsoil anomalies characterized by high resistivity.

The electrodes employed and tested are those available at the Laboratory of Engineering Geology, University of Florence. To try to answer the research questions above mentioned, the study has been carried out in terms of analysis of the apparent resistivity (ρ_a) data to avoid introducing further errors/approximations caused by the inversion procedure applied to reconstruct the real subsoil resistivity.

Section II illustrates the tested electrodes and the measurement campaign, while Section III describes the obtained results. The discussion of the results and the conclusions of the work are provided in Sections IV and V, respectively.

II. Materials and Methods

The goal of ERT method is to assess the subsurface resistivity of the soil through measurements taken on the ground surface. The acquired resistivity values provided by the instrument do not yet represent the true resistivity of the subsurface.
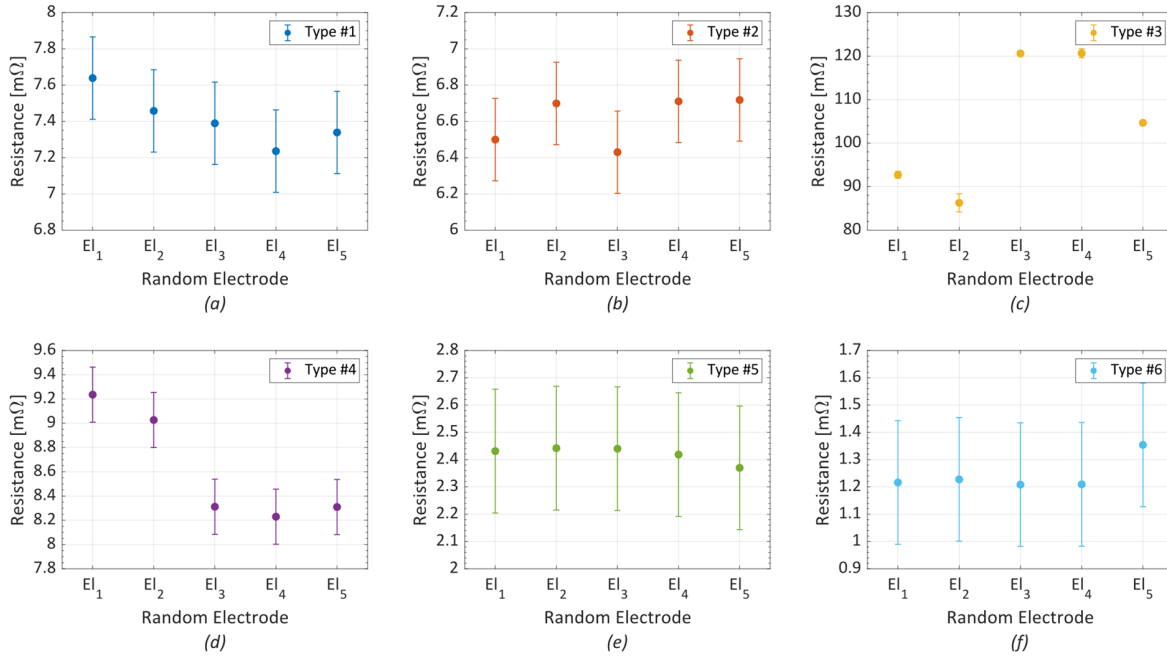
Fig. 1. Measured resistance values for the five electrodes type #. The extension of the bars stands for the expanded uncertainty with 95% confidence level calculated by (1)–(5). (a) Electrode Type #1. (b) Electrode Type #2. (c) Electrode Type #3. (d) Electrode Type #4. (e) Electrode Type #5. (f) Electrode Type #6.

Instead, resistivity data are "apparent" values representing the "global" complex mean resistivity of the ground. The acquired measurements depend on the electrode configuration during the measurement campaign. The "apparent" resistivity should then be postprocessed by adequate "inversion" algorithms to reconstruct a 2-D or 3-D model of the subsurface resistivity. The "inversion" procedure involves complex algorithms (including, for instance, convolutional neural network [35], U-Net deep neural network [36], Gauss–Newton method [37], and algebraic reconstruction technique [38]) and several approximations. For this reason, the following analysis deals only with the acquired values of the apparent resistivity in order to avoid the introduction of further uncertainties, dealing only with those caused by the different a/φ ratio tested.

Six distinct types of electrodes were tested having diameters (φ) from 4 to 16 mm (see specific data in Table I). Five of them were made of stainless steel and one of graphite. The electrical resistance (R_{el}) of each one was measured by using a calibrated 6(1/2) -Digit Bench Multimeter by Keithley (model DMM6500). Because of the extremely low resistance value of the electrodes, a four-wire resistance measurement method was implemented, with an instrument resolution of 1 $\mu\Omega$ and a measurement range of 1 Ω.

For every type of electrode under test, five samples have been randomly selected to measure their electrical resistance, with 100 consecutive readings acquired for every sample under repeatability conditions. Considering the random electrode j of type #k, the instrument provides $\overline{R_{k\_j}}$ and σ_{k_j}, which represent the mean value and the standard deviation of the electrical resistance, respectively. The average of the mean and standard deviation values for each electrode type is summarized in Table I, while all the measured resistances with associated expanded uncertainty u_{k_j} are reported in Fig. 1

in the case of 95% confidence level. More specifically, the expanded uncertainty has been evaluated in compliance with the ISO Guide to the Expression of Uncertainty in Measurement (GUM) [39] procedure according to the following steps:

$$s_{A_{k\_j}} = \frac{\sigma_{k\_j}}{\sqrt{N}} = \frac{\sigma_{k\_j}}{\sqrt{100}} \tag{1}$$

$$s_{B_{k\_j}} = \frac{\text{acc}_{k\_j}}{\sqrt{3}} \tag{2}$$

$$u_{\text{comb}_{k\_j}} = \sqrt{s_{A_{k\_j}}^2 + s_{B_{k\_j}}^2} \tag{3}$$

where $u_{\text{comb}_{k\_j}}$ is the combined uncertainty in the resistance measurement in the case of random electrode j of type #k, which depends on $s_{A_{k\_j}}$, Type A uncertainty arises from multiple measurements, and $s_{B_{k\_j}}$, Type B uncertainty due to systematic errors such as calibration errors and instrument inaccuracy. The latter is calculated based on the multimeter accuracy, which, according to the manufacturer and under the specified operating conditions, and it is given by

$$\text{acc}_{k\_j} = \pm(0.0085\%\text{Reading} + 0.02\%\text{range}). \tag{4}$$

Then, the expanded uncertainty u_{k_j} has been calculated considering a coverage factor $k = 1.96$ due to the assumptions of standardized normal distribution and 95% confidence level as the best tradeoff between precision and width of the confidence interval

$$u_{k\_j} = k \cdot u_{\text{comb}_{k\_j}}. \tag{5}$$

All the evaluated uncertainties are reported in Fig. 1 as the length of the vertical error bar for each of the five random electrodes and for each type. Furthermore, the average uncertainty on all the electrodes is reported in Table I for each type. As can be noted in Fig. 1, all the stainless-steel electrodes show compatible resistance values, while the variability of the graphite electrodes is much higher.

TABLE I
TESTED ELECTRODES: THEIR DIAMETER (φ), MATERIAL, MEAN RESISTANCE VALUE, AND RESISTANCE STANDARD DEVIATION

| Electrode	Diameter [mm]	Length [cm]	Material	Mean Resistance [mΩ]	Resistance standard deviation [μΩ]	Resistance uncertainty [μΩ]
Type #1	4	15	Stainless-steel 304	7.412190	35.32617	± 227.14
Type #2	5	20	Stainless-steel 316	6.611448	35.83094	± 227.07
Type #3	6	10	Graphite	104.9849	4.72655	± 971.01
Type #4	8	60	Stainless-steel	8.622593	35.33339	± 227.26
Type #5	10	30	Stainless-steel	2.420343	41.65082	± 226.71
Type #6	16	40	Stainless-steel	1.243107	40.69388	± 226.59
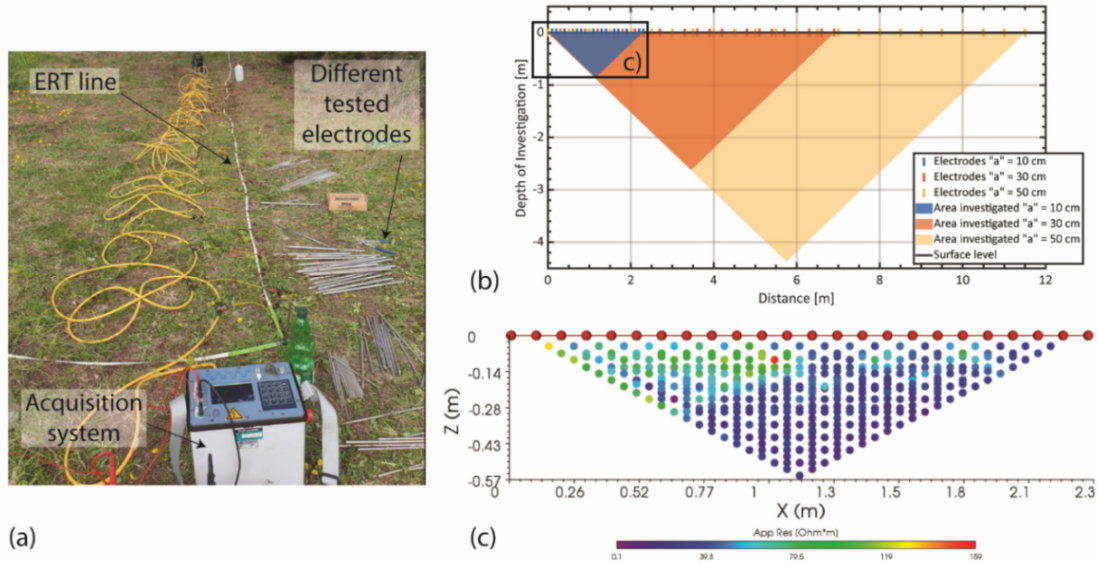
Fig. 2. (a) Photograph of the experimental setup with the acquisition system, the ERT line, and the different electrodes tested. (b) Schematic representation of the subsoil investigated by the PD-ERT with an "a" = 10 cm (blue), 30 cm (orange), and 50 cm (dark yellow). The area investigated using "a" = 1 m was not shown to avoid losing figure resolution in the first meters of the ERT. (c) Real distribution of the acquired apparent resistivity data for the DD-ERT with "a" = 10 cm: each line of dots is placed at the so-called pseudo-depth (see the text for more details).

The acquisitions were carried out on 30 March 2023 in the garden outside the Engineering Geology Laboratory of the University of Florence [see Fig. 2(a)], an almost homogeneous site. The weather was sunny with a mean temperature of 19 °C, a variation of 2 °C between the first and last acquisition, and a relative humidity of 58%. Data of temperature and humidity were recorded by a Davis weather station permanently installed near the Engineering Geology Laboratory of the University of Florence and located few meters north from the ERT test. The apparent resistivity (ρ_a) was acquired using a ten-channel receiver SyscalPro by Iris [visible in Fig. 2(a)], equipped with 24 electrodes. Given the different lengths of the tested electrodes (see Table I), to avoid a too long active electrode [26] possibly generating artifacts as discussed in Section I, each electrode was inserted in the soil for few centimeters (2–3 cm) so that the active length was the same in all the ERT acquisitions.

Two different array topologies [the PD and the dipole–dipole (DD)] and four different interelectrode distances "a" (10, 30, 50, and 100 cm) were tested for each electrode type for a total of 48 ERT surveys. For more information about DD and PD arrays, see [12]. Each PD-ERT and DD-ERT allowed to measure 986 and 806 values of apparent resistivity (ρ_a), respectively. The spatial distribution in the subsoil of the PD-ERT acquired measurements for an "a" distance of 10, 30, and 50 cm is shown in Fig. 2(b). The area investigated using an "a" distance of 1 m was not shown to avoid losing resolution in the figure. The subsoil investigated by the DD-ERT has the same shape as the PD-ERT one, but lower depth.

In Fig. 2(c), the 806 apparent resistivity acquisitions for the DD-ERT with "a" = 10 cm are shown, and each line of dots represents the so-called pseudo-depth as in [11]. It is important to remember here, in fact, that an increase in the electrode spacing "a" allows to reach a higher depth of investigation. but losing resolution (i.e., the distance between two depths of acquisition is higher).

Table II shows the electrode's spacing-to-diameter ratio (a/φ) and the electrode's diameter-to-spacing ratio (φ/a) for each electrode type and interelectrode distances "a" value.

TABLE II

ELECTRODE'S SPACING-TO-DIAMETER RATIO AND ELECTRODE'S DIAMETER-TO-SPACING RATIO FOR EACH TESTED ELECTRODE. "a" IS THE ELECTRODES' SPACING AND φ IS THE DIAMETERS OF EACH ELECTRODE TYPES AS LISTED IN TABLE I

Electrode	"a" = 10 cm		"a" = 30 cm		"a" = 50 cm		"a" = 100 cm	
	a/φ	φ/a	a/φ	φ/a	a/φ	φ/a	a/φ	φ/a
Type #1	25.0	0.040	75.0	0.013	125.0	0.008	250.0	0.004
Type #2	20.0	0.050	60.0	0.017	100.0	0.010	200.0	0.005
Type #3	16.7	0.060	50.0	0.020	83.3	0.012	166.7	0.006
Type #4	12.5	0.080	37.5	0.027	62.5	0.016	125.0	0.008
Type #5	10.0	0.100	30.0	0.033	50.0	0.020	100.0	0.010
Type #6	6.3	0.160	18.8	0.053	31.3	0.032	62.5	0.016

The minimum and maximum φ/a tested are 0.4% (for electrode type #1 and "a" = 100 cm) and 16% (considering electrode type #6 and "a" = 10 cm), respectively.

During field measurements, the electrode resistance (R_{el}) becomes a part of the soil-electrode contact resistance (R_{s-el}), i.e., the resistance that affects the input voltage and thus the input current. R_{s-el} is an indicator of the goodness of the soil-electrode coupling, i.e., lower the values better the coupling. The instrument employed in this study acquires, at each acquisition, the contact resistance between the two current electrodes (A and B, so in the following, it is called R_{AB}) that is the sum of the two soil-electrode coupling resistances (R_{s-elA} and R_{s-elB}) and the resistance of the soil in between the two electrodes. Thus, according to [25], it is possible to write the following overdetermined linear system:

$$X * R_{s-el} = R_{AB} \qquad (6)$$

where X is an (m, n) matrix of the form

$$X = \begin{bmatrix} 1 & 1 & 0 & \cdots \\ 0 & 1 & 1 & \cdots \\ 1 & 0 & 1 & \cdots \\ \vdots & \vdots & \vdots & \ddots \end{bmatrix} \qquad (7)$$

with m (rows) the number of acquisitions and n (columns) the number of electrodes (equal to 24 for the DD-ERT in this application). In each row of (7), there are only two $x_{ij} = 1$, and all the others are equal to 0, i.e., 1 is assigned to those positions associated with the two electrodes that in that acquisition are working as current electrodes (e.g., in the first row of the matrix X, the elements $x_{11} = x_{12} = 1$ mean that electrodes 1 and 2 are working as A and B, while in the second row, $x_{22} = x_{23} = 1$, so electrodes 2 and 3 are the current electrodes, and so on).

R_{s-el} is the vector $(1, n)$ of the soil-electrode contact resistances, expressed in [kΩ], to be determined, of the form

$$R_{s-el} = \begin{bmatrix} R_{s-el,1} \\ R_{s-el,2} \\ R_{s-el,3} \\ \vdots \\ R_{s-el,24} \end{bmatrix} \qquad (8)$$

and R_{AB} is the vector $(1, m)$ of the contact resistances, expressed in [kΩ] and acquired by the SyscalPro instrument

at each acquisition ($m = 806$ in this application), of the form

$$R_{AB} = \begin{bmatrix} R_{A=1,B=2} \\ R_{A=2,B=3} \\ R_{A=1,B=3} \\ \vdots \end{bmatrix}. \qquad (9)$$

Being X and R_{AB} known, it is possible to solve the system with the last squares methods and obtain R_{s-el} as

$$R_{s-el} = \text{inv}(X' * X) * X' * R_{AB}. \qquad (10)$$

Therefore, according to [25] and (10), R_{s-el} of the 24 electrodes involved in each DD-ERT was calculated. It was not possible to calculate R_{s-el} for the PD-ERTs because all the measures have in common the electrode 25. Thus, the $X' * X$ matrix is a 25 × 25 matrix with a determinant equal to 0 having values along the diagonal, the last column, and the last row.

As said in Section I, it is known that the resistivity is dependent on the temperature of both the soil and the pore fluid [1], [40]. Nevertheless, there are studies (see, for example, [41]) that show as a soil temperature variation of few degrees results in negligible resistivity variations at shallow depth (up to 40 cm) and do not have effects at higher depth. Therefore, in the following analyses, ERT data were not corrected for the soil temperature variation.

III. RESULTS

Apart for electrode type #3 (the one in graphite), R_{s-el} of the stainless-steel electrodes involved in each ERT was in the range 0.1–0.6 kΩ, as shown in Fig. 3. Considering that R_{el} of each electrode type as illustrated in Fig. 1 is approximately five orders of magnitude lower than R_{s-el}, it is possible to state that R_{s-el} is linked only to the local soil conditions and the differences in the electrode materials do not influence the coupling, and therefore, all the other considerations will be drawn in the following. In Figs. 4 and 5, for each of the four tested interelectrode distances "a" (the four panels) and for each electrode type expressed as its a/φ value (different colors), the acquired ρ_a values are shown as a function of the pseudo-depth [11] for the DD and PD arrays, respectively. The global legend above [Fig. 4(a)–(d)] is common to each of the four panels and it illustrates electrode type #. A similar meaning has the global legend located above (Fig. 5).
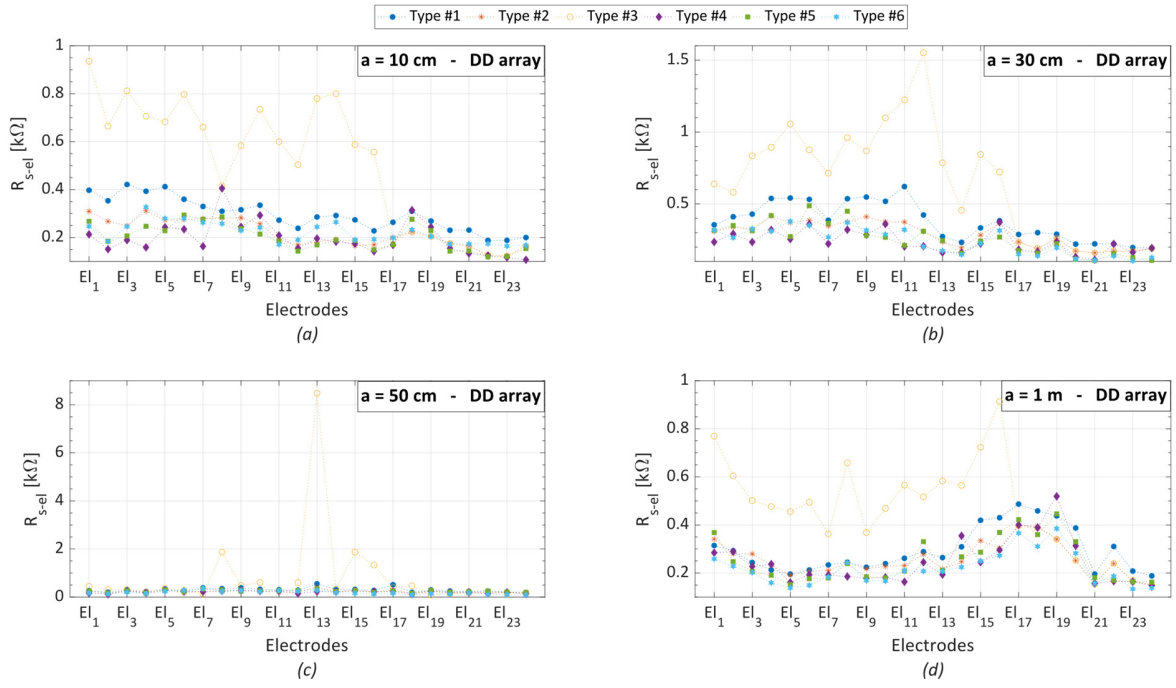
Fig. 3. R_{s-el} of the 24 electrodes of each type involved: (a) "a" $= 10$ cm, (b) "a" $= 30$ cm, (c) "a" $= 50$ cm, and (d) "a" $= 1$ m.
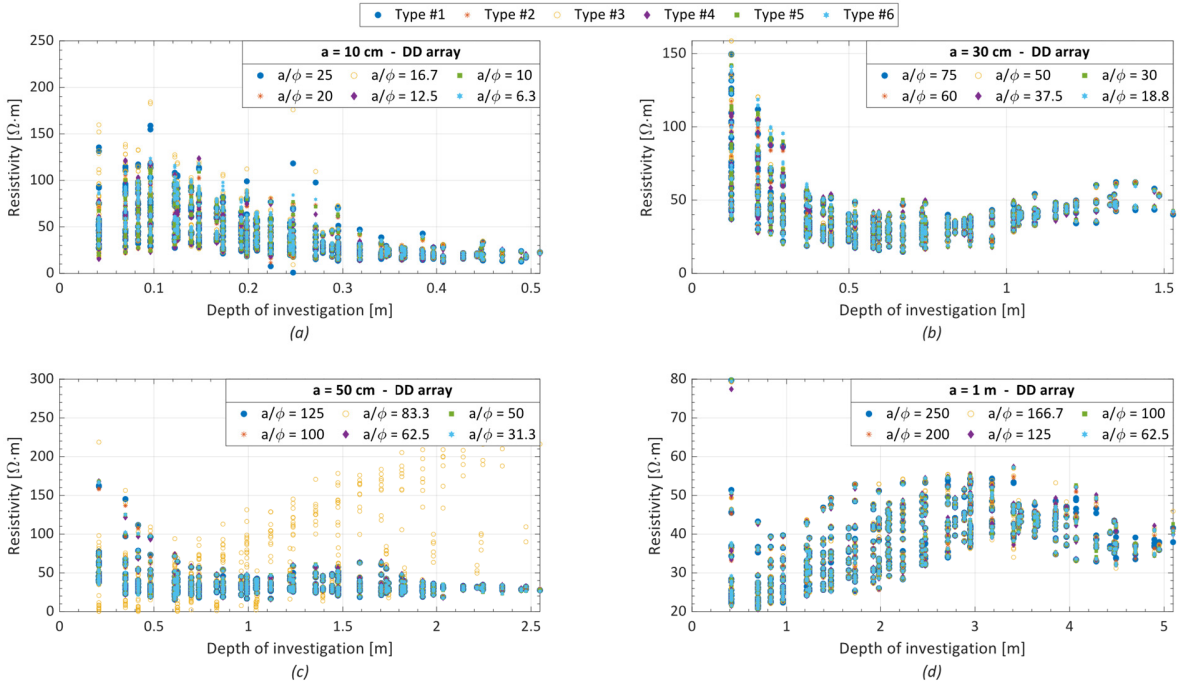

Fig. 4. Apparent resistivity acquired in the case of DD-ERT as a function of depth of investigation and the electrode's spacing-to-diameter ratio (a/φ). The interelectrode distance is (a) "a" $= 10$ cm, (b) "a" $= 30$ cm, (c) "a" $= 50$ cm, and (d) "a" $= 1$ m.

Figs. 4 and 5, in agreement with [30], show that the a/φ value does not influence the acquired apparent resistivity ρ_a when the interelectrode distance "a" is set equal to 1 m. This means that all the tested electrodes, apart electrode type 6, has a/φ value higher than 100 (i.e., the condition of $\varphi/a \leq 1\%$ suggested in [30] for long electrodes is satisfied). This is clearer in the case of PD array (see Fig. 5), but it can be easily appreciated also in the case of DD array (see Fig. 4). In the DD array (see Fig. 4), the influences of the a/φ ratio

is visible in the first four to five pseudo-depths when "a" is set equal to 30 cm (i.e., all the a/φ are lower than 100) and 50 cm (i.e., only one a/φ is higher than 100), and up to the last ten pseudo depths when the interelectrode distance is set equal to 10 cm (i.e., all the a/φ values are lower than 100).

For the PD array (see Fig. 5), the behavior is comparable, with a higher variation at shallow depth and when the a/φ ratio is lower than 80 (that corresponds to $\varphi/a \leq 1.25\%$).
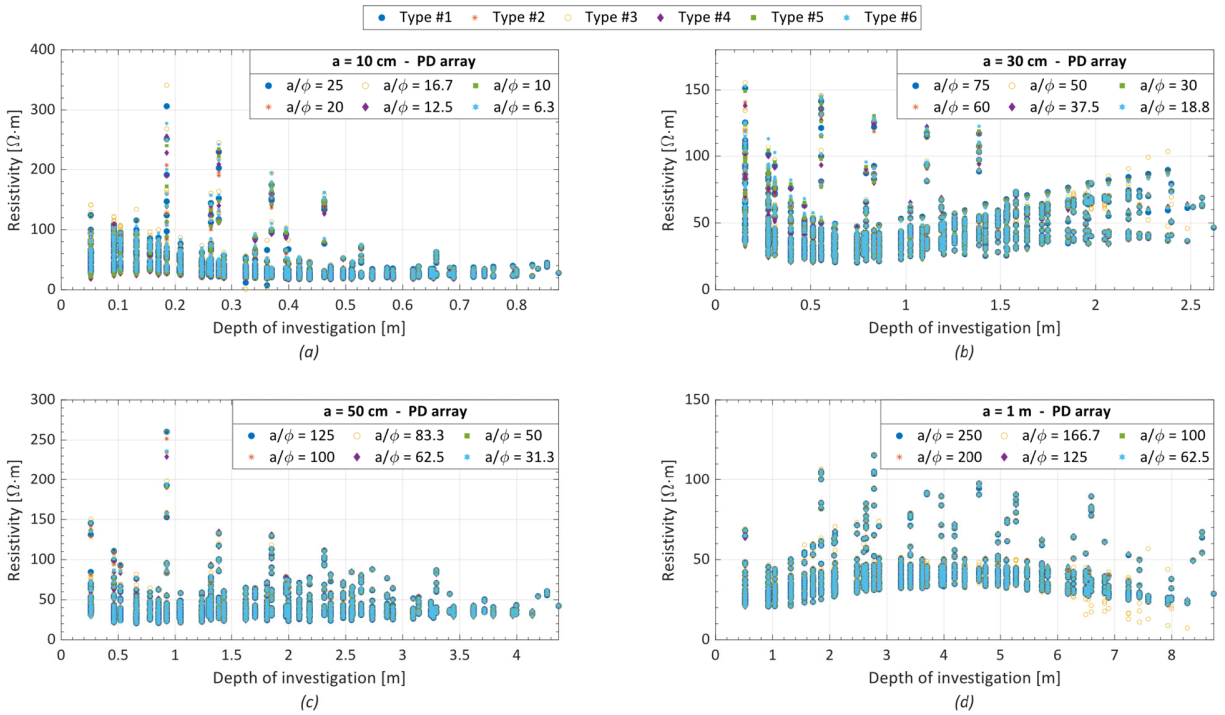
Fig. 5.   Apparent resistivity acquired in the case of PD-ERT as a function of depth of investigation and the electrode's spacing-to-diameter ratio (a/φ). The interelectrode distance is (a) "a" = 10 cm, (b) "a" = 30 cm, (c) "a" = 50 cm, and (d) "a" = 1 m.

IV. DISCUSSION

To understand the influence of the electrode spacing to electrode diameter ratio a/φ on the acquired apparent resistivity ρ_a, the standard deviation of all the measurements acquired with the five different stainless-steal electrodes and for each distance "a," and thus for each point of the subsoil, has been calculated. As recalled in the introduction and shown in Fig. 2, different values of the interelectrode distance "a" allow to obtain ERT profiles of different lengths and thus to reach different depths, i.e., the subsoil distribution of the acquisition is that shown in Fig. 2(c), but the distances between acquisition increase with the increase of "a." Thus, data acquired with different "a" cannot be directly compared because they are not referred to the same subsoil portion. Nevertheless, the number of pseudo-depth levels is influenced by the integer parameter "n" that indicates how many interelectrode spacings "a" there are between the current electrodes and voltage electrodes (e.g., for a DD with $A = \text{El}_1$, $B = \text{El}_2$, $M = \text{El}_3$, and $N = \text{El}_4$, "n" is equal to 1, i.e., the distance between B and M is equal to "a," while for a DD with $A = \text{El}_1$, $B = \text{El}_2$, $M = \text{El}_4$, and $N = \text{El}_5$, "n" is equal to 2, i.e., the distance between B and M is two times "a." For more specific information, see also [20], [21], and [22].

Therefore, the pseudo-depth level [i.e., each dot line in Fig. 2(c)] can be seen as a relative depth that allows to compare data measured with a different "a" value. Fig. 6 shows that the standard deviations as a function of the relative depth (from 0, i.e., the surface, to 1, i.e., the maximum depth reached by the DD and PD arrays that are about 5 and 9 m, respectively), which means as a function of the pseudo-depth level. In particular, chosen a value of "a" (different colors in Fig. 6), each point of the graphs in Fig. 6 represents a
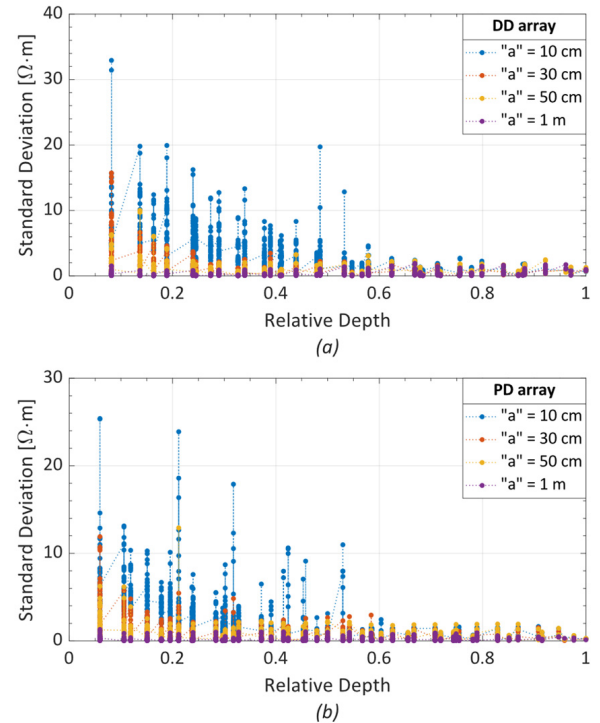

Fig. 6.   Standard deviation of the ρ_a values, acquired by the five different stainless-steal electrodes, shown as a function of the relative depth of investigation for different interelectrode distances in the case of (a) DD and (b) PD array.

specific acquisition quadripole [i.e., each of the dots shown in Fig. 2(c)] and indicates the standard deviation of the apparent resistivity associated with that subsoil position [shown in
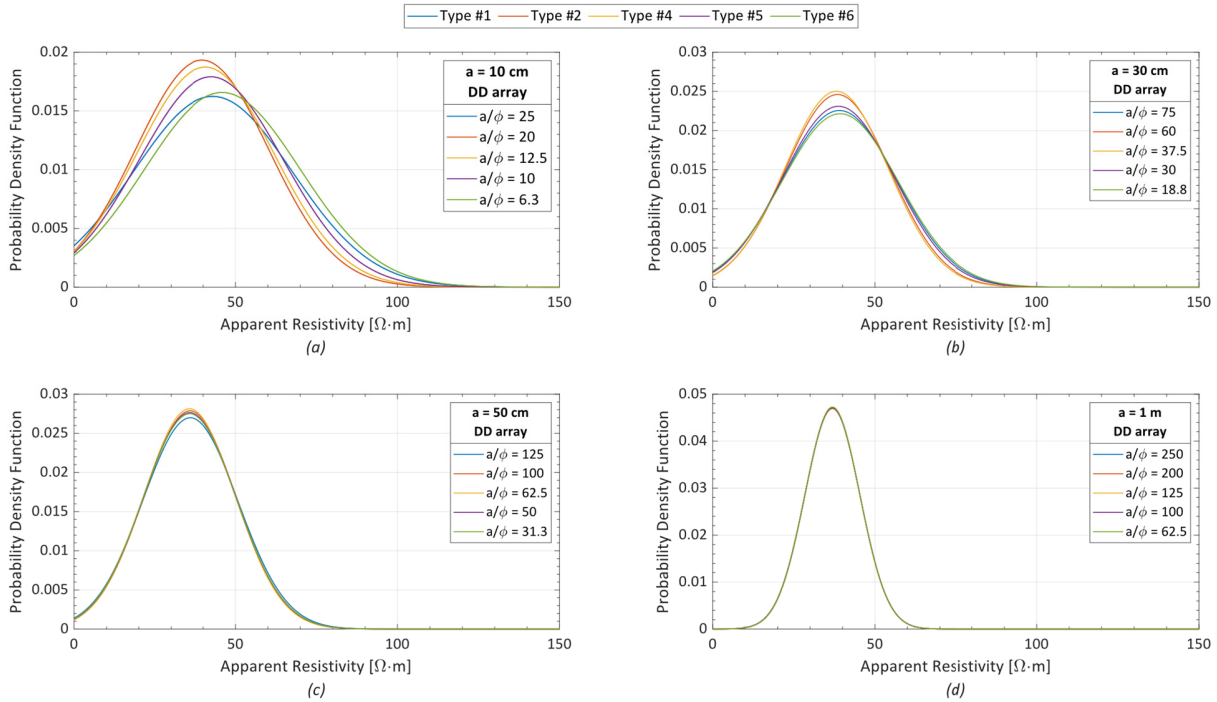
Fig. 7. Probability distribution of the acquired data in the case of DD array, considering various electrode's spacing-to-diameter ratio (a/φ) and different interelectrode distances are (a) 10 cm, (b) 30 cm, (c) 50 cm, and (d) 1 m.

Fig. 2(c)] and acquired by means of the five stainless-steal electrodes.

It is possible to observe the high variability of the standard deviation when "a" = 10 cm (blue dots) up to a relative depth of 0.6 for both DD and PD arrays. This means that the a/φ ratio lower than 25 (that corresponds to $\varphi/a \geq 4\%$) has a major influence on the measures up to a real depth of three times the interelectrode distance. The variability in the standard deviation is still visible when "a" = 30 cm and "a" = 50 cm and reach its minimum (it seems to disappear) for "a" = 1 m, i.e., when a/φ value is higher than 100, and thus, the condition of $\varphi/a \leq 1\%$ suggested in [30] for long electrodes is satisfied. In general, for both DD and PD arrays, the standard deviation does not seem to be influenced by the interelectrode distance (and thus by the a/φ ratio) at a relative depth higher than 0.6.

Moreover, considering "a" = 10 cm [the blue trends in Fig. 6(a) and (b)] and fixing a relative depth, it is possible to observe that the standard deviation has a great variability (e.g., for the first relative depth, the standard variation ranges from 4 to 34 Ωm). This means that some acquisitions at the same depth are more subject to the a/φ ratio variation, and thus, the acquired apparent resistivity values are more spread. Checking for the acquisitions with a greater standard deviation, it is possible to note that they are located at the beginning of the ERT in correspondence with a shallow resistive anomaly [higher acquired apparent resistivity values shown in green in Fig. 2(c)]. This result, in addition to what highlighted previously, indicates also that the a/φ ratio lower than 25 (that corresponds to a $\varphi/a \geq 4\%$) has a major influence in

those applications where the targets are resistive anomalies (e.g., in achaeo-geophysics).

To better emphasize this concept, Table III summarizes some of the measurements characterized by the highest and lowest standard deviation values for a certain interelectrode distance "a" and a specific depth of investigation. The table includes the acquisition number, the measuring electrodes, and the measured resistivity considering the five stainless-steel types. The mean value and the standard deviation of the measured apparent resistivity are also included. Looking at the table, it is clear how the highest standard deviation values are always linked to high measured resistivity, while the lowest variability occurs when the measured apparent resistivity is low. This is true regardless of the interelectrode distance "a," the depth of investigation, and the array type. As a matter of fact, similar values are also obtained for all the other acquisitions, the other depths, and the PD array. Thus, they are not included for the sake of brevity. Table III also verifies the concept that emerged from Fig. 6 that the greater variability between the electrode types (and thus the greater impact of the electrode's diameter and a/φ ratio) is shown at shallow depth, while the effect tends to decrease when the depth of investigation increases.

Nevertheless, from Fig. 6 and Table III, the information about the a/φ ratio is lost. Therefore, to better understand the a/φ ratio influence, the probability distributions of the measured apparent resistivity ρ_a with respect to different interelectrode distances (each subplot), considering various electrode's spacing-to-diameter ratio (a/φ) with different colors, is shown for the DD and PD arrays in Figs. 7 and 8,
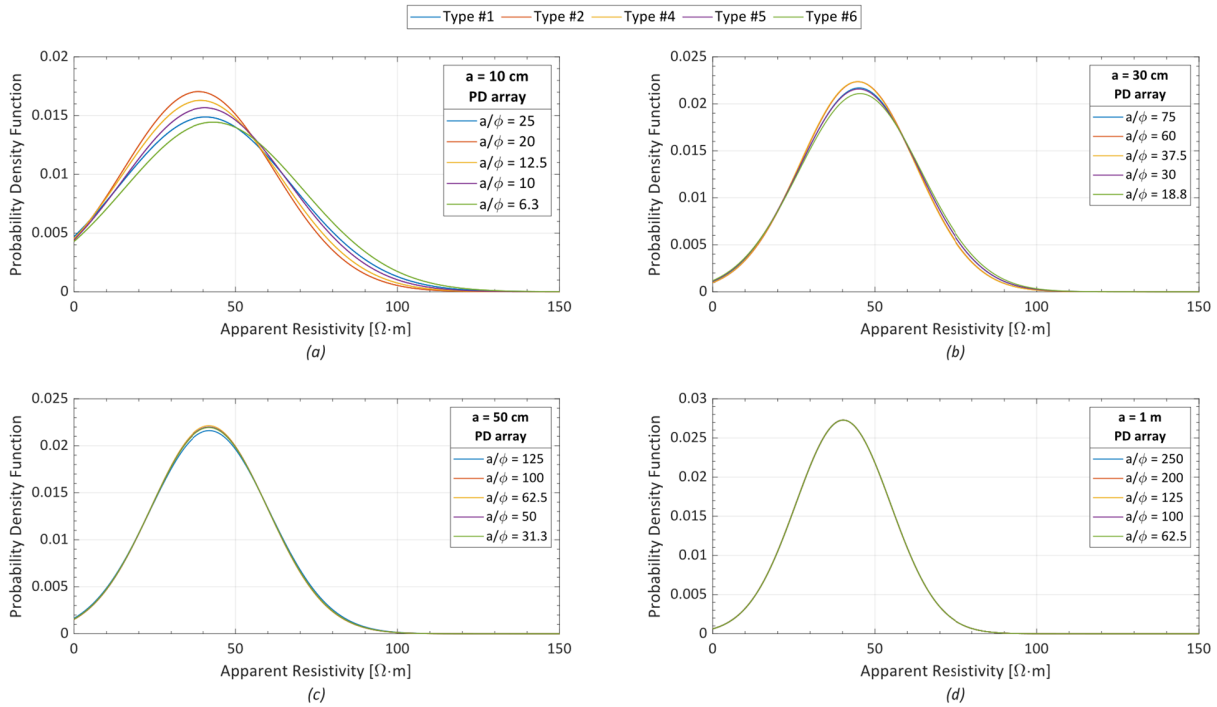
Fig. 8. Probability distribution of the acquired data in the case of PD array, considering that various electrode's spacing-to-diameter ratio (a/φ) and different interelectrode distances are (a) 10 cm, (b) 30 cm, (c) 50 cm, and (d) 1 m.

TABLE III
SUMMARY OF SOME OF THE ACQUIRED VALUES IN THE CASE OF DD-ERT CHARACTERIZED BY THE HIGHEST AND LOWEST STANDARD DEVIATION VALUES FOR A CERTAIN DEPTH AND A CERTAIN "a"

| "a" | Depth [cm] | Acq | Measuring Electrodes | | | | Apparent Resistivity ρ_a [Ωm] | | | | | Mean Value | Standard Deviation |
			A	B	M	N	Type #1	Type #2	Type #4	Type #5	Type #6		
10 cm	4.16	1	El_1	El_2	El_3	El_4	135.463	78.050	52.345	58.314	86.838	82.202	32.930
		337	El_{10}	El_{11}	El_8	El_9	52.311	60.006	50.515	50.995	50.665	52.898	4.036
	6.97	2	El_1	El_2	El_4	El_5	114.837	85.455	66.413	81.353	107.535	91.119	19.811
		374	El_{11}	El_{12}	El_{14}	El_{15}	43.905	39.784	42.538	40.311	49.821	43.272	4.025
	9.62	304	El_9	El_{10}	El_{13}	El_{14}	158.842	116.392	118.417	106.992	123.583	124.845	19.930
	9.62	483	El_{14}	El_{15}	El_{18}	El_{19}	51.602	45.974	46.939	45.637	50.203	48.071	2.675
30 cm	12.48	230	El_7	El_8	El_9	El_{10}	131.614	114.955	100.476	124.206	137.110	121.672	14.474
		480	El_{14}	El_{15}	El_{12}	El_{13}	37.119	38.342	37.034	39.304	40.142	38.388	1.357
50 cm	34.85	407	El_{12}	El_{13}	El_9	El_{10}	145.280	137.022	121.488	124.977	125.190	130.791	10.006
		626	El_{18}	El_{19}	El_{15}	El_{16}	30.932	31.154	30.612	30.674	30.618	30.798	0.238

respectively. In each subplot, the same color indicates the same electrode type # according to the legend common to all the subplots above (Figs. 7 and 8). Results for DD and PD arrays are in accordance and do not seem to show significant differences.

If the a/φ ratio does not influence the acquired ρ_a, what is expected is that the probability distributions of data acquired by means of different a/φ values are comparable, which means that the dataset has the same median and standard deviation. This is what is shown in Figs. 7(d) and 8(d), i.e., for "a" = 1 m. The probability distributions of all the tested a/φ are perfectly comparable. This result suggests that

the relation $\varphi/a \leq 1\%$ suggested in [30] for long electrodes can be increased up to $\varphi/a \leq 1.6\%$, which corresponds to $a/\varphi \geq 62.5$. Moreover, considering the results in Figs. 7(c) and 8(c), it seems that the a/φ ratio can be reduced up to 31.5 (i.e., $\varphi/a \leq 3.2\%$). The probability distribution of the measured data when "a" = 50 cm, in fact, shows negligible differences and can be considered in agreement for the different a/φ tested.

An $a/\varphi = 31.5$ means that in the case of electrodes with a diameter of 4 mm, the "a" distance should be more than 12.6 cm, and in the case of electrodes with a diameter of 16 mm, it should be more than 50.4 cm. It is not unusual to

employ these "a" distances in agro-geophysics [8] or achaeo-geophysics [21], [29], where the target is shallow, and a high resolution is needed [29]. Moreover, considering that in micro-geophysics the electrode's diameter range between 1.5 and 2.0 mm [29], an $a/\varphi = 31.5$ means that the inter-electrode distance "a" should range between 4.7 and 6.3 cm, respectively.

These results are also confirmed by the probability distribution of the data acquired with "a" = 30 cm (i.e., Fig. 7(b) in the case of DD array and Fig. 8(b) in the case of PD array): the first differences in the probability distribution, i.e., the influence of the a/φ ratio, are evident for a/φ values lower than 30 (i.e., the red and light blue curves). Finally, the probability distribution of the data acquired with "a" = 10 cm [that corresponds to $\varphi/a \geq 4\%$ and it is shown in Figs. 7(a) and 8(a)] shows the highest variability (different mean values and standard deviations) and it is not possible to assess which of them is not affected by the a/φ value. On the contrary, it is possible to assess with a quite high degree of confidence that this variability is not influenced by the active electrode length higher than the maximum suggested by [27]. These authors, in fact, assessed that in the inversion of micro-ERT profiles, electrodes cannot be approximated as point electrodes but must be considered with their real geometry if the ratio between the active electrode and "a" is not kept well below 0.2. This limit means 2 and 6 cm for "a" = 10 cm and "a" = 30 cm, respectively.

Nevertheless, for operational reasons (i.e., to avoid introducing differences in the different ERTs) in this study, the active electrode length was kept equal for all the ERTs (i.e., about the minimum "a" tested) and the analysis was conducted in terms of apparent resistivity and not real resistivity, assuming that, if an effect of the active electrode was really present, it has to be the same in all the acquisitions.

V. Conclusion

This study was carried out to fill a gap in the literature about small-scale ERT and, in particular, about the influence on the acquired data of the ratio between the interelectrode distance "a" and the electrode's diameter (the a/φ ratio). Overall, six distinct types of electrodes were employed. The tested electrodes were stainless-steal or graphite stakes with a diameter ranging from 4 to 16 mm. To avoid considering the active electrode length and the generation of possible artifacts induced by not accounting for the real electrode shape, the analysis was conducted in terms of apparent resistivity, and the electrodes were inserted in the soil for few centimeters.

First, this study shows that the soil-electrode resistance (R_{s-el}) is influenced only by the local soil conditions and the differences in the electrode materials do not influence the coupling. Thus, the differences in the acquired data are not linked to the electrode material but to other factors. Moreover, the analyses of the acquired data with respect to the depth, to their standard deviations, and to their probability distributions highlighted how the a/φ ratio has to be ≥ 31.5 (i.e., $\varphi/a \leq 3.2\%$) to avoid artifacts in the acquired data and, thus, in the inverted models.

A potential bias of the work could be seen in not having repeated the test in different environments. Acquired data are of course site-dependent, but the purpose of the work was not to investigate the specificities of the site, but to see possible effects of the a/φ ratio used. Thus, the analysis was conducted in terms of apparent resistivity and not in terms of inverted resistivity model, and an almost homogeneous site was chosen. Nevertheless, the presence of an unknown shallow resistive anomaly has demonstrated the need to use the correct a/φ ratio to avoid possible artifacts, especially in the presence of resistive targets. This result is of particular interest for those applications, such as the archaeo-geophysics, which are conducted primarily to identify resistive anomalies. To evaluate the real influence of resistivity anomalies, possible future analyses could be conducted in a controlled (i.e., artificial) environment as well as numerical forward modeling. Another potential bias could be seen in the selection of the instrumentation, but according to the results [25], acquisition by means of different instruments is comparable.

A limitation of the proposed method lies in having tested only two arrays, the DD and PD ones. Further studies will therefore have to be conducted, considering other commonly used arrays such as the Wenner, the Wenner–Schlumberger, and the gradient [2], [18]. Another drawback of the proposed methodology could be linked to the tested materials: even if stainless steel is the most employed one [2] and the results of this study show that the differences in the electrode materials do not influence the acquired apparent resistivity, other materials could be investigated to better generalized the obtained results.

References

[1] D. S. Parasnis, *Principles of Applied Geophysics*, 4th ed. London, U.K.: Chapman & Hall, 1986.

[2] M. H. Loke, J. E. Chambers, D. F. Rucker, O. Kuras, and P. B. Wilkinson, "Recent developments in the direct-current geoelectrical imaging method," *J. Appl. Geophys.*, vol. 95, pp. 135–156, Aug. 2013, doi: 10.1016/j.jappgeo.2013.02.017.

[3] F. Dong, C. Tan, J. Liu, Y. Xu, and H. Wang, "Development of single drive electrode electrical resistance tomography system," *IEEE Trans. Instrum. Meas.*, vol. 55, no. 4, pp. 1208–1214, Aug. 2006, doi: 10.1109/TIM.2006.877751.

[4] A. Binley et al., "The emergence of hydrogeophysics for improved understanding of subsurface processes over multiple scales," *Water Resour. Res.*, vol. 51, no. 6, pp. 3837–3866, Jun. 2015, doi: 10.1002/2015WR017016.

[5] G. Baccani et al., "The reliability of muography applied in the detection of the animal burrows within river levees validated by means of geophysical techniques," *J. Appl. Geophys.*, vol. 191, Aug. 2021, Art. no. 104376, doi: 10.1016/j.jappgeo.2021.104376.

[6] V. Pazzi, S. Morelli, and R. Fanti, "A review of the advantages and limitations of geophysical investigations in landslide studies," *Int. J. Geophys.*, vol. 2019, pp. 1–27, Jul. 2019, doi: 10.1155/2019/2983087.

[7] Z. Ren et al., "Development of a novel linear ERT sensor to measure surface deposits," *IEEE Trans. Instrum. Meas.*, vol. 68, no. 3, pp. 754–761, Mar. 2019, doi: 10.1109/TIM.2018.2853380.

[8] D. Vanella, S. R. Peddinti, and I. Kisekka, "Unravelling soil water dynamics in almond orchards characterized by soil-heterogeneity using electrical resistivity tomography," *Agricult. Water Manage.*, vol. 269, Jul. 2022, Art. no. 107652, doi: 10.1016/j.agwat.2022.107652.

[9] C. Tan, Y. Shen, K. Smith, F. Dong, and J. Escudero, "Gas–liquid flow pattern analysis based on graph connectivity and graph-variate dynamic connectivity of ERT," *IEEE Trans. Instrum. Meas.*, vol. 68, no. 5, pp. 1590–1601, May 2019, doi: 10.1109/TIM.2018.2884548.

[10] S. V. Calcina, P. Parisi, and L. Piroddi, "3D electrical resistivity tomography: A diagnostic tool for the inspection of submerged foundations of civil infrastructures," in *Proc. 21st Int. Conf. Comput. Sci. Appl. (ICCSA)*, Sep. 2021, pp. 225–233, doi: 10.1109/ICCSA54496.2021.00039.

[11] K. Li, S. Yue, F. Dong, and Y. Xu, "Fault diagnosis of ERT system based on choquet integral," in *Proc. IEEE Int. Instrum. Meas. Technol. Conf. (I2MTC)*, May 2023, pp. 1–6, doi: 10.1109/I2MTC53148.2023.10175936.

[12] L. Ciani et al., "Comparing the effects of GPS error on different electrical resistivity tomography arrays for archeological investigations," *IEEE Trans. Instrum. Meas.*, vol. 70, pp. 1–12, 2021, doi: 10.1109/TIM.2020.3021513.

[13] X. Deng, Y. Chen, Z. Yan, and Z. Wei, "AC impedance model of array electrodes in multisensor fusion system for two-phase flow measurement," *IEEE Trans. Instrum. Meas.*, vol. 59, no. 6, pp. 1722–1726, Jun. 2010, doi: 10.1109/TIM.2009.2028209.

[14] K. Gao, Z. Cui, Z. Xia, and H. Wang, "Electrical resistance tomography using high and low conductivity calibration," in *Proc. IEEE Int. Instrum. Meas. Technol. Conf. (I2MTC)*, May 2020, pp. 1–6, doi: 10.1109/I2MTC43012.2020.9128990.

[15] F. Dong, Y. Xu, L. Hua, and H. Wang, "Two methods for measurement of gas-liquid flows in vertical upward pipe using dual-plane ERT system," *IEEE Trans. Instrum. Meas.*, vol. 55, no. 5, pp. 1576–1586, Oct. 2006, doi: 10.1109/TIM.2006.881564.

[16] T. H. S. Sousa, E. D. L. B. Camargo, A. R. C. Martins, C. Biasi, A. C. B. C. F. Pinto, and R. G. Lima, "In vivo measurements for construction an anatomical thoracic atlas for electrical impedance tomography (EIT): Methods for EIT regularizations," in *Proc. IEEE Int. Instrum. Meas. Technol. Conf. (I2MTC)*, May 2014, pp. 802–805, doi: 10.1109/I2MTC.2014.6860853.

[17] A. Cultrera and L. Callegaro, "Electrical resistance tomography of conductive thin films," *IEEE Trans. Instrum. Meas.*, vol. 65, no. 9, pp. 2101–2107, Sep. 2016, doi: 10.1109/TIM.2016.2570127.

[18] B. Zhou and T. Dahlin, "Properties and effects of measurement errors on 2D resistivity imaging surveying," *Near Surf. Geophysics*, vol. 1, no. 3, pp. 105–117, Aug. 2003, doi: 10.3997/1873-0604.2003001.

[19] G. A. Oldenborger, P. S. Routh, and M. D. Knoll, "Sensitivity of electrical resistivity tomography data to electrode position errors," *Geophys. J. Int.*, vol. 163, no. 1, pp. 1–9, Oct. 2005, doi: 10.1111/j.1365-246X.2005.02714.x.

[20] S. Razafindratsima and J.-F. Lataste, "Estimation of the error made in Pole–Dipole electrical resistivity tomography depending on the location of the remote electrode: Modeling and field study," *J. Appl. Geophys.*, vol. 100, pp. 44–57, Jan. 2014, doi: 10.1016/j.jappgeo.2013.10.008.

[21] V. Pazzi et al., "Analysis of the influence of the GPS errors occurred while collecting electrode coordinates on the electrical resistivity of tumuli," *Sensors*, vol. 20, no. 10, p. 2966, May 2020, doi: 10.3390/s20102966.

[22] M. Catelani et al., "Effects of inaccurate electrode positioning in subsurface resistivity measurements for archeological purposes," in *Proc. IEEE Int. Instrum. Meas. Technol. Conf. (I2MTC)*, May 2021, pp. 1–6, doi: 10.1109/I2MTC50364.2021.9459977.

[23] G. Patrizi et al., "Analysis of non-ideal remote pole in electrical resistivity tomography for subsurface surveys," in *Proc. IEEE Int. Instrum. Meas. Technol. Conf. (I2MTC)*, May 2022, pp. 1–5, doi: 10.1109/I2MTC48687.2022.9806650.

[24] D. La Brecque, W. Daily, and P. Adkins, "Systematic errors in resistivity measurement systems," in *Proc. Symp. Appl. Geophys. Eng. Environ. Problems*, Jan. 2007, pp. 1153–1160, doi: 10.4133/1.2924620.

[25] A. D. Parsekian et al., "Comparing measurement response and inverted results of electrical resistivity tomography instruments," *J. Environ. Eng. Geophys.*, vol. 22, no. 3, pp. 249–266, Sep. 2017, doi: 10.2113/jeeg22.3.249.

[26] C. Verdet, Y. Anguy, C. Sirieix, R. Clément, and C. Gaborieau, "On the effect of electrode finiteness in small-scale electrical resistivity imaging," *Geophysics*, vol. 83, no. 6, pp. EN39–EN52, Nov. 2018, doi: 10.1190/geo2018-0074.1.

[27] J. Ochs and N. Klitzsch, "Considerations regarding small-scale surface and borehole-to-surface electrical resistivity tomography," *J. Appl. Geophys.*, vol. 172, Jan. 2020, Art. no. 103862, doi: 10.1016/j.jappgeo.2019.103862.

[28] T. Ingeman-Nielsen, S. Tomašković ová, and T. Dahlin, "Effect of electrode shape on grounding resistances—Part 1: The focus-one protocol," *Geophysics*, vol. 81, no. 1, pp. WA159–WA167, Jan. 2016, doi: 10.1190/geo2015-0484.1.

[29] P. L. Cosentino, P. Capizzi, R. Martorana, P. Messina, and S. Schiavone, "From geophysics to microgeophysics for engineering and cultural heritage," *Int. J. Geophys.*, vol. 2011, pp. 1–8, Jan. 2011, doi: 10.1155/2011/428412.

[30] C. Rücker and T. Günther, "The simulation of finite ERT electrodes using the complete electrode model," *GEOPHYSICS*, vol. 76, no. 4, pp. F227–F238, Jul. 2011, doi: 10.1190/1.3581356.

[31] M. Ronczka, C. Rücker, and T. Günther, "Numerical study of long-electrode electric resistivity tomography— Accuracy, sensitivity, and resolution," *Geophysics*, vol. 80, no. 6, pp. E317–E328, Nov. 2015, doi: 10.1190/geo2014-0551.1.

[32] M. Masi and V. Pazzi, "Portable low-cost measurement system development for self-potential (SP) monitoring in severe environmental conditions," in *Proc. 32 Nat. Congr. (GNGTS)*, 2013, pp. 138–143.

[33] D. Epishkin and N. Zorin, "Measurement of noise characteristics of graphite electrodes in the field and comparison with other types of non-polarizing electrodes," in *Proc. 25th EM Induction Workshop*, 2022, pp. 1–3.

[34] T. Dahlin and V. Leroux, "Improvement in time-domain induced polarization data quality with multi-electrode systems by separating current and potential cables," *Near Surf. Geophys.*, vol. 10, no. 6, pp. 545–565, Dec. 2012, doi: 10.3997/1873-0604.2012028.

[35] F. Li, C. Tan, and F. Dong, "Electrical resistance tomography image reconstruction with densely connected convolutional neural network," *IEEE Trans. Instrum. Meas.*, vol. 70, pp. 1–11, 2021, doi: 10.1109/TIM.2020.3013056.

[36] Q. Guo, B. Liu, Y. Wang, and D. He, "A deep learning inversion method for 3-D electrical resistivity tomography based on neighborhood feature extraction," *IEEE Sensors J.*, vol. 23, no. 16, pp. 18550–18558, Aug. 2023, doi: 10.1109/JSEN.2023.3293205.

[37] M. H. Loke and R. D. Barker, "Rapid least-squares inversion of apparent resistivity pseudosections by a quasi-Newton method1," *Geophys. Prospecting*, vol. 44, no. 1, pp. 131–152, Jan. 1996, doi: 10.1111/j.1365-2478.1996.tb00142.x.

[38] Z. Xu, J. Huang, Y. Jiang, B. Wang, Z. Huang, and M. Soleimani, "An image reconstruction algorithm for a 12-electrode capacitively coupled electrical resistance tomography system under 2-electrode excitation strategy," *IEEE Trans. Instrum. Meas.*, vol. 70, pp. 1–11, 2021, doi: 10.1109/TIM.2021.3098388.

[39] *Uncertainty of Measurement—Part 3: Guide to the Expression of Uncertainty in Measurement*, Standard ISO/IEC Guide 98-3, International Organization for Standardization (ISO), 2008.

[40] K. Hayley, L. R. Bentley, M. Gharibi, and M. Nightingale, "Low temperature dependence of electrical resistivity: Implications for near surface geophysical monitoring," *Geophys. Res. Lett.*, vol. 34, no. 18, Sep. 2007, Art. no. L18402, doi: 10.1029/2007gl031124.

[41] W. Nijland, M. van der Meijde, E. A. Addink, and S. M. de Jong, "Detection of soil moisture and vegetation water abstraction in a Mediterranean natural area using electrical resistivity tomography," *Catena*, vol. 81, no. 3, pp. 209–216, Jun. 2010, doi: 10.1016/j.catena.2010.03.005.

Lorenzo Ciani (Senior Member, IEEE) received the M.S. degree in electronic engineering and the Ph.D. degree in industrial and reliability engineering from the University of Florence, Florence, Italy, in 2005 and 2009, respectively.

He is currently an Associate Professor with the Department of Information Engineering, University of Florence. He has authored or coauthored more than 220 peer-reviewed journals and conference papers. His current research interests include system reliability, availability, maintainability and safety, reliability evaluation test and analysis for electronic systems and devices, fault detection and diagnosis, and electrical and electronic instrumentation and measurement.

Dr. Ciani is a member of the IEEE IMS TC-32 Fault Tolerant Measurement Systems. He received the 2015 IEEE I&M Outstanding Young Engineer Award for "his contribution to the advancement of instrumentation and measurement in the field of reliability analysis." He is a Senior Area Editor of IEEE TRANSACTION ON INSTRUMENTATION AND MEASUREMENT and an Associate Editor of IEEE ACCESS.
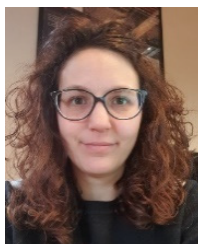
Gabriele Patrizi (Member, IEEE) received the master's degree (cum laude) in electronic engineering and the Ph.D. degree in industrial and reliability engineering from the University of Florence, Florence, Italy, in 2018, and 2022, respectively.

He is currently a Post-Doctoral Research Fellow in the field of instrumentation and measurement and an Adjunct Lecturer of electric measurements with the University of Florence. In 2022, he joined the Institute of Electronic Packaging Technology (IAVT), Dresden Technical University, Dresden, Germany, as a Visiting Post-Doctoral Researcher. His research interests include life-cycle reliability, condition monitoring for fault diagnosis of electronics, data-driven prognostic and health management, and instrumentation and measurement for reliability analysis.

Dr. Patrizi has been an Associate Editor of IEEE TRANSACTIONS ON INSTRUMENTATION AND MEASUREMENT (TIM) since 2023. He was a recipient of the "2023 Best Dissertation Award" from IEEE IMS.

Riccardo Fanti received the M.Sc. degree in geological sciences from the University of Florence, Florence, Italy, in 1994, and the Ph.D. degree in engineering geology, geomorphology and groundwater hydrology from the University of Perugia, Perugia, Italy, in 1999.

He is currently an Associate Professor of engineering geology with the Department of Earth Sciences, University of Florence. He has authored or coauthored more than 150 peer-reviewed journal articles and conference papers. His current research interests include the study of landslide and erosion phenomena, the development of warning and monitoring systems for disaster prevention, methods for the assessment of geological-environmental hazards and risks, and the modeling of flow and transport in aquifer systems.

Dr. Fanti is a member of the UNESCO Chair on Prevention and Sustainable Mitigation of Geo-hydrological Hazards and a member of the Academic Senate at University of Florence.

Agnese Innocenti received the B.S. degree in geology and the M.S. degree in engineering geology from the Department of Earth Science, University of Florence, Florence, Italy, in 2016 and 2020, respectively. She is currently pursuing the Ph.D. degree in applied geophysics with the Department of Agriculture, Food, Environment and Forestry, University of Florence.

Her current research interests include the use of geophysical methods to study small-scale features in the shallow and deep subsurface, the study of landslides through the application of geophysical and geotechnical techniques, and the modeling of landslide slopes.

Ms. Innocenti won the David Giuntini prize for the best master's thesis in 2020.

Veronica Pazzi received the M.Sc. degree in environmental engineering and the Ph.D. degree in civil and environmental engineering from the University of Florence, Florence, Italy, in 2007 and 2011, respectively.

From 2011 to 2021, she was a Post-Doctoral Researcher with the Department of Earth Sciences, University of Florence. From 2021 to 2024, she was a Researcher at the University of Trieste, Trieste, Italy. Since 2022, she has been the Scientific Officer of the EGU NH3—Landslides and Avalanches subdivision. Since 2024, she has been an Associate Professor at the University of Florence. She has authored or coauthored about 120 peer-reviewed journal articles and conference papers. Her research interests include geophysical investigations, especially electrical resistivity and passive seismic methods, applied to engineering geology, applied seismology, and archeological/cultural heritage problems and hazard, vulnerability, and risk assessment.

Dr. Pazzi is an Editor of NHESS, *Landslides*, the *International Journal of Disaster Risk Reduction*, and the *International Journal of Geophysics*.